

## Accepted Manuscript

Title: Perspectives on the effect of sulfur on the hydrocarbonaceous overlayer on iron Fischer-Tropsch catalysts

Authors: Robbie Warringham, Alisha L. Davidson, Paul B. Webb, Robert P. Tooze, Stewart F. Parker, David Lennon



PII: S0920-5861(18)30969-6  
DOI: <https://doi.org/10.1016/j.cattod.2019.02.035>  
Reference: CATTOD 11987

To appear in: *Catalysis Today*

Received date: 19 October 2018  
Revised date: 28 January 2019  
Accepted date: 16 February 2019

Please cite this article as: Warringham R, Davidson AL, Webb PB, Tooze RP, Parker SF, Lennon D, Perspectives on the effect of sulfur on the hydrocarbonaceous overlayer on iron Fischer-Tropsch catalysts, *Catalysis Today* (2019), <https://doi.org/10.1016/j.cattod.2019.02.035>

This is a PDF file of an unedited manuscript that has been accepted for publication. As a service to our customers we are providing this early version of the manuscript. The manuscript will undergo copyediting, typesetting, and review of the resulting proof before it is published in its final form. Please note that during the production process errors may be discovered which could affect the content, and all legal disclaimers that apply to the journal pertain.

**Paper for submission to:**

Catalysis Today

(Special Issue: New Opportunity and Challenges in Energy and Environmental Catalysis)

**Draft:**

28<sup>th</sup> January 2019

## **Perspectives on the effect of sulfur on the hydrocarbonaceous overlayer on iron Fischer-Tropsch catalysts**

Robbie Warringham<sup>a</sup>, Alisha L. Davidson<sup>a</sup>, Paul B. Webb<sup>b</sup>, Robert P. Tooze<sup>c</sup>, Stewart F. Parker<sup>d</sup>, David Lennon<sup>a\*</sup>

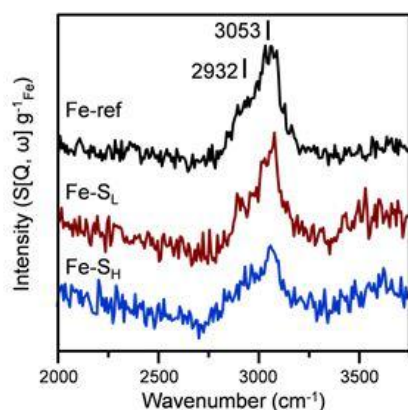
- a. School of Chemistry, Joseph Black Building, University of Glasgow, Glasgow, G12 8QQ, UK
- b. School of Chemistry, University of St Andrews, St Andrews, KY16 9ST, UK
- c. Group Technology, Research and Technology, Sasol Ltd
- d. ISIS Facility, STFC Rutherford Appleton Laboratory, Chilton, Didcot, Oxon OX11 0QX, UK

### **\*Corresponding author**

Professor David Lennon CChem, FRSC  
School of Chemistry  
Joseph Black Building  
The University of Glasgow  
Glasgow, G12 8QQ  
U.K.

Email: David.Lennon@glasgow.ac.uk  
Telephone: +44-141-330-4372

## Graphical abstract



## Highlights

- An ambient pressure test reaction leads to the formation of a hydrocarbonaceous overlayer;
- Post-reaction XRD, TPO and INS analysis indicates the presence of sulfur to impede the supply of surface hydrogen;
- INS identifies a diminished hydrocarbonaceous fingerprint as a function of sulfur loading;
- The nature of the hydrocarbonaceous overlayer is sensitive to sulfur loading.

## Abstract

Fischer-Tropsch synthesis (FTS) is commonly viewed as an alternative approach to the production of diesel fuels via sources independent of crude oil. The adaptability of the FTS process allows for the selective production of shorter chain  $C_2$  to  $C_6$  hydrocarbons and has the potential to be a legitimate source of useable chemical feedstocks with high value to the chemical manufacturing industry. Interestingly, although recognised as a poison in most catalytic systems, small amounts of sulfur in iron-based FTS catalysts has been demonstrated to promote catalyst reducibility and activity towards shorter chain hydrocarbons. However, it is not known what impact sulfur has on the formation of hydrocarbonaceous surface species that have been proposed to play a pivotal role in the mediation of reactants during iron FTS. Here we apply ambient pressure CO hydrogenation at 623 K on a selection of sulfur

promoted iron FTS catalysts to investigate the effect of sulfur content on hydrocarbonaceous species formation. For the first time, we report the application of inelastic neutron scattering to quantify the presence of hydrocarbonaceous species under the presence of sulfur promotion. In combination with temperature programmed oxidation, X-ray diffraction, and Raman spectroscopy, we observe how low sulfur loadings (<700 ppm) perturb carbon and hydrogen retention levels. The results indicate that the presence and nature of the hydrocarbonaceous overlayer is sensitive to sulfur loading, with the reported loss in catalytic activity at high loadings correlating with the attenuation of hydrocarbonaceous surface species.

### Abbreviations

FTS, Fischer-Tropsch synthesis; INS, Inelastic neutron scattering; TPO, Temperature programmed oxidation; XRD, X-ray diffraction; TEM, Transmission electron microscopy; MS, Mass spectrometer; WHSV, Weight hourly space velocity; sccm, Standard cubic centimetres per minute.

### Keywords

Fischer-Tropsch, sulfur promotor, iron catalyst, inelastic neutron scattering, hydrocarbonaceous overlayer

### 1.0 Introduction

With the increasing scarcity and volatility of obtaining crude oil for our primary fuel demands, there is a concerted effort globally to seek alternatives that alleviate our dependency. Fischer-Tropsch synthesis (FTS) is one example of a technology in use today that can provide an alternative production route for fuel independently from crude oil sources<sup>1, 2</sup>. Therefore, FTS can be regarded as a stopgap technology that can bridge the transition from crude oil derived products to the world scale commercialisation of established biomass technologies. Briefly FTS is a metal catalysed polymerisation reaction which converts synthesis gas (syngas, CO and H<sub>2</sub>) to a range of hydrocarbon products that can be further processed towards diesel fuel and high value chemicals<sup>3-6</sup>. As the syngas feedstock can be derived from sources such as natural gas, coal and biomass, and in

combination with recent legislation that prevents the flaring of natural gas, there is a real incentive to utilise this approach to replace crude oil-based technologies<sup>7-12</sup>.

An interesting facet of FTS is the degree of chemical control one can exert over the product slate through the promotion of the catalyst material; in effect increasing the value and flexibility of the synthesis. For example, in iron-based FTS, alkali metals such as sodium and potassium can enhance activity, lower selectivity to methane and accelerate carbidisation but may also cause increased formation of carbon<sup>3, 13-20</sup>. The use of sulfur as a promoter is much less commonly applied for the primary reason that it is a well-known poison<sup>21, 22</sup>. Appealingly, however, it has been proposed that the inclusion of small amounts of sulfur have a promoting effect on iron-based FTS. Specifically, it has been observed to effect catalyst reducibility and enhance activity whilst driving product selectivity towards olefins<sup>17, 23, 24</sup>, thereby providing higher value to the chemical manufacturing industry. In 1999 a study by Bromfield and Coville reported a peak in catalytic activity during FTS (523 K, H<sub>2</sub>: CO = 2:1, 8 bar) and a higher selectivity towards C<sub>2</sub> to C<sub>6</sub> hydrocarbons with a sulfur content of *ca.* 500 ppm<sup>23</sup>. Increasing sulfur content beyond this value had a detrimental effect on the catalytic activity. The higher selectivity to olefins has also been reported by other groups with several operating hypotheses proposed<sup>17, 25-27</sup>. For example, in 2013 De Jong and co-workers suggest this distinct selectivity is a result of sulfur weakening the iron-carbon bond at the surfaces of the iron carbide nanoparticles, facilitating the formation of shorter chain hydrocarbons<sup>17</sup>. Similarly, Kritzinger proposes that sulfur poisons highly active sites responsible for hydrogenating surface olefin species<sup>27</sup>. Zhou *et al* propose that sulfur may initially increase carbon deposition but when sulfur levels are increased past a certain value this will decrease<sup>28</sup>. Yuan and co-workers suggest that sulfur as a sole promoter may decrease catalytic activity in comparison to an un-promoted sample and that the inclusion of a second promoter, an alkali metal, is required for the increase in activity<sup>29</sup>.

Recent studies from this group have pioneered the application of inelastic neutron scattering (INS) to investigate the hydrocarbonaceous species retained on industrially and laboratory reacted iron-based FTS catalysts<sup>30-34</sup>. INS is particularly advantageous for the study of coked materials as it does not suffer from the optical selection rules that govern IR and Raman spectroscopies<sup>35</sup>. Further, the technique is uniquely sensitive to hydrogenous vibrations and therefore able to identify the presence of sp<sup>3</sup> and sp<sup>2</sup> hybridised carbon atoms<sup>35</sup>. These INS studies report on the presence of a surface hydrocarbonaceous species,

consisting of aliphatic carbon with residual aromatic character that forms during the reaction. It is suggested these species constitute an overlayer that could play a role in defining the probable distribution of sites on an iron-based FTS catalyst<sup>34</sup>.

With respect to the proposed surface effects of sulfur promotion, and the potential this could have in disrupting the formation of a hydrocarbonaceous overlayer, here we report a preliminary study of two sulfur promoted iron-based FTS catalysts by INS. Sulfur loadings were chosen to encompass above and below the optimal value of 500 ppm proposed by Bromfield and Coville<sup>23</sup>. Samples were exposed to reaction conditions used in the previous INS investigations of FTS catalysts (ambient pressure CO hydrogenation at 623 K) for varying lengths of time to temporally analyse the formation of the hydrocarbonaceous species in the presence of sulfur. Characterisation was accomplished by temperature programmed oxidation (TPO), X-ray diffraction (XRD), and Raman spectroscopy as well as INS analysis. This approach allows the speciation and quantification of the carbonaceous and hydrogenous species present in the sample. As with previous reports, we find the inclusion of sulfur delays the reduction of the starting iron oxide phase and increases carbidisation, particularly at higher loadings. Moreover, the high sulfur loading reduces the intensity of hydrogenous modes measured by INS, indicating an inverse correlation between the presence of sulfur and the development of the hydrocarbonaceous overlayer.

## 2.0 Experimental

### 2.1. Catalyst preparation

The iron oxide catalyst sample used for this investigation was prepared using the co-precipitation of iron nitrate (Sigma Aldrich, 99.99 %) and sodium carbonate (Sigma Aldrich, 99.99 %). The preparative procedure utilizes a batch reactor apparatus for reproducible sample synthesis and is described elsewhere<sup>33,34</sup>. The procedure produces hematite ( $\alpha$ -Fe<sub>2</sub>O<sub>3</sub>) with a surface area of 70.8 m<sup>2</sup>g<sup>-1</sup> and an absence of promoters/modifiers (sample code Fe-ref). For the sulfur promoted samples, the same preparative method for Fe-ref was followed but with ammonium sulphate (Sigma Aldrich, 99.99%) used in place of the sodium carbonate. The concentration of ammonium sulphate solution was varied in order to alter the final sulfur concentration of each sample. Two samples containing low (Fe-S<sub>L</sub>) and high (Fe-S<sub>H</sub>) sulfur concentrations were prepared. All samples were ground and sieved to a particle size range of 250-500  $\mu$ m. Sulfur content was quantified using inductively coupled plasma optical emission spectrometry (ICP).

## 2.2. Micro-reactor measurements

Reaction testing was performed at ambient pressure using a catalyst test line composed of 1/8 in. diameter stainless steel Swagelok tubing, a description of which can be found elsewhere<sup>33, 34</sup>. Approximately 40 mg of sample was loaded into a 1/4 in. quartz tube reactor and plugged with quartz wool. The reactor is housed within a tube furnace (Carbolite MTF 10/15/30) equipped with PID control. A thermocouple is positioned within the catalyst bed to ensure accurate temperature readings during measurement. For CO hydrogenation reactions, gas flows of CO (3.35 sccm, 99.5%, CK gas), H<sub>2</sub> (6.75 sccm, 99.9%, BOC) and He (21.25 sccm, 99.9%, BOC) are established over the bypass before introduction over the catalyst (total weight hourly space velocity (WHSV) of 60.8 h<sup>-1</sup>). All gas flows were monitored using an in-line quadrupole mass spectrometer (Hiden Analytical, HPR-20) attached to the reactor exit line via a differentially-pumped, heated quartz capillary. Mass traces for sulfur compounds, *e.g.* hydrogen sulphide, were measured but not observed during reaction testing. The sample was subjected to a temperature ramp of 5 K min<sup>-1</sup> to 623 K and held for a pre-determined length of time, after which the reactant flows were halted, and the temperature cooled to ambient under the helium carrier gas. For ex situ characterisation, reacted samples were subjected to a passivation procedure involving a gradual increase in the oxygen levels up until atmospheric levels (*i.e.* 20% O<sub>2</sub> in the gas feed)<sup>36</sup>.

## 2.3. Inelastic neutron scattering measurements

For INS measurements, approximately 10 g of catalyst was loaded into an Inconel reactor cell and attached to a custom-built sample preparation rig<sup>37</sup>. For CO hydrogenation measurements, the iron oxide catalyst was heated to 623 K at 5 K min<sup>-1</sup> under a flow of CO (75 sccm, CK Gas, 99.9%) and H<sub>2</sub> (150 sccm, CK Gas, 99.9 %) in a carrier gas (He, 600 sccm, CK Gas, 99.9%, total WHSV of 1.47 h<sup>-1</sup>) and held at temperature for a pre-determined length of time. The gas products were analysed by an in-line mass spectrometer (Hiden Analytical, HPR20 QMS Sampling System). Note that the MS instrument utilised for these scaled-up reaction measurements at the ISIS Facility is uncalibrated at the time of measurement, therefore the gas traces are a qualitative representation of the reaction profiles. Once the specific reaction had finished, the reactant gases were stopped, and the sample allowed to cool to room temperature under the carrier gas. The reactor cell was isolated and placed in an argon-filled glove box (MBraun UniLab MB-20-G, [H<sub>2</sub>O] <1 ppm, [O<sub>2</sub>] <2 ppm) before being loaded into an aluminium sample holder that is sealed via an indium wire gasket<sup>38</sup>. All

INS measurements were performed using the MAPS direct geometry spectrometer<sup>35</sup>. Spectra were recorded at 20 K at an incident neutron energy of 600 meV and 250 meV using the A-chopper package. Quantification of the  $\nu(\text{C-H})$  feature obtained by INS was achieved following a calibration protocol described elsewhere<sup>39</sup>.

## 2.4 Pre- and post-reaction analysis

TPO of the micro-reactor samples was performed post-reaction in situ whilst the large-scale reactor samples were analysed ex situ. Oxygen (5% in He, 70 sccm, BOC Ltd, 99.5%) was introduced to the sample (ca. 40 mg) and the reactor heated to 1173 K at 5 K min<sup>-1</sup> using the mass spectrometer to monitor the eluting gases. Quantification of the CO<sub>2</sub> peak area was achieved by measuring the CO<sub>2</sub> response from the in situ TPO of known masses of graphite (Sigma Aldrich, 99.9%)<sup>40</sup>. Powder XRD was performed using a Siemens D5000 diffractometer, with a Cu K $\alpha$  radiation in Bragg-Brentano geometry in the 2 $\theta$  range 5-85° (step size 0.02° s<sup>-1</sup>). For in situ XRD studies ca. 200 mg of ground sample was placed in an Anton Paar XRK-900 reaction chamber with a K-type thermocouple housed in the reaction chamber. Temperature control was maintained by an Anton Paar TCU 750 temperature control unit equipped with a PID control (Eurotherm 2604). A H<sub>2</sub>:CO mixture (2:1, 10 sccm, CK Gases, 99.5%) in carrier gas (Ar, 20 sccm, BOC Ltd, 99.9%) was introduced via 1/4 in. Swagelok tube gas lines, with a thermocouple positioned within the catalyst bed to ensure accurate temperature reading during measurements. The sample was heated to 623 K at 5 K min<sup>-1</sup> and maintained at 623 K for 24 h. Diffractograms were recorded every hour. Reflections were assigned based on the following reference diffraction patterns;  $\alpha$ -Fe<sub>2</sub>O<sub>3</sub>, JCPDS #13-534; Fe<sub>3</sub>O<sub>4</sub>, JCPDS #19-629;  $\alpha$ -Fe, JCPDS #6-696; Fe<sub>5</sub>C<sub>2</sub>, JCPDS #36-1248; Fe<sub>3</sub>C, JCPDS #32-0772. Ex situ Raman scattering was performed using a Horiba Jobin Yvon LabRam HR confocal Raman microscope and a 532 nm laser source at <20 mW power. Measurements were taken for approximately 5 min.

## 3.0 Results

### 3.1 Fresh catalyst characterisation

The freshly prepared Fe-ref, Fe-S<sub>L</sub> and Fe-S<sub>H</sub> samples were preliminarily characterized using ICP, XRD, and Raman to establish the sulfur content and its effect on the iron oxide crystallinity. Estimation of the sulfur concentration by ICP was successful in the case of Fe-S<sub>H</sub>, indicating 700 ppm present, but was unable to quantify the sulfur loading in Fe-S<sub>L</sub> (targeted value of 154 ppm); this sulfur level is below the sensitivity of the ICP instrumentation utilised (<300 ppm). Note that the iron concentrations of all samples were identical. Assessment of



the crystallinity of the sulfur loaded samples by XRD indicates iron oxide is in the  $\alpha$ -Fe<sub>2</sub>O<sub>3</sub> phase, identical with the Fe-ref sample (**Figure 1a**). Changes in the crystallographic matrix of the hematite induced by the presence of sulphur are not expected owing to the low levels. Other studies involving the addition of low quantities of sulfur have also shown, through XRD, that addition of the promoter has made no structural changes to the hematite<sup>29</sup>. The similarities in the diffractograms of the sulfur-modified samples with Fe-ref would indicate there to be a homogeneous distribution of the sulfur. Raman spectra (**Figure 1b**) of all three samples are characteristic of  $\alpha$ -Fe<sub>2</sub>O<sub>3</sub><sup>41</sup>.

## 3.2 Micro-reactor studies

### 3.2.1 CO hydrogenation test reaction

Previous studies have reported the application of ambient pressure CO hydrogenation at elevated temperature as a representative test reaction to assess the surface chemistry of an Fe FTS catalyst relevant to FTS conditions *i.e.* CO/H<sub>2</sub> dissociation and C-C/C-H bond formation.<sup>31, 42</sup> This approach was utilized here to assess the impact of sulfur inclusion on these processes. Recent work by Mejía *et al* has highlighted the importance of a reduction step for cobalt based FTS catalysts prior to reaction.<sup>43</sup> However, a H<sub>2</sub>-pretreatment step has been shown to be detrimental to catalytic performance of iron based catalysts, as it causes an increase in carbon retention resulting from the increased presence of metallic iron which facilitates carbidisation.<sup>32</sup> Therefore, no pre-treatment of the catalyst was used in this instance.

In comparison to Fe-ref,<sup>33</sup> the reaction profiles for Fe-S<sub>L</sub> and Fe-S<sub>H</sub> are identical (**Figure 2**). The three stages identified previously are also present;<sup>33</sup> Stage I - the reduction of  $\alpha$ -Fe<sub>2</sub>O<sub>3</sub> to Fe<sub>3</sub>O<sub>4</sub> by CO, Stage II - the simultaneous production of CO<sub>2</sub>, CH<sub>4</sub> and H<sub>2</sub>O and consumption of CO and H<sub>2</sub> at 623 K, Stage III – decrease in product yield towards steady-state operation. It is noted in separate measurements that the mass traces for sulfur monoxide and sulfur dioxide (*m/z* 48 and 64 respectively), possible products from the oxidation of sulfur species, were monitored during the reaction but were not observed. CO conversion profiles for Fe-S<sub>L</sub> and Fe-S<sub>H</sub> approximate to <1% during Stage III of the reaction coordinate, similar to the Fe-ref sample<sup>33</sup> (**Figure 3a,b**). Olefin formation was not explicitly observed under the stated reaction conditions; it is anticipated that elevated pressures are necessary to induce such product formation of low loading S modified Fe catalysts. As noted elsewhere,<sup>31</sup> ambient pressure CO hydrogenation is favoured as a test reaction for the INS based studies

considered here as it prevents the build-up of high molecular weight hydrocarbons that would otherwise compromise the INS spectra. The emphasis of the current series of FTS INS studies<sup>30-34</sup> is to examine the surface chemistry of the Fe/CO/H<sub>2</sub> reaction system. Moreover, it is noted that a 6 h test period is not sufficient when testing for catalyst deactivation but was selected as a suitable reaction period in the first instance for this preliminary study for direct comparison to the Fe-ref sample<sup>33</sup>.

### 3.2.2 Post-reaction characterisation

The in situ XRD profiles of Fe-S<sub>L</sub> and Fe-S<sub>H</sub> during ambient pressure CO hydrogenation indicate the reduction of  $\alpha$ -Fe<sub>2</sub>O<sub>3</sub> to Fe<sub>3</sub>O<sub>4</sub> and the formation of iron carbides (**Figure 4**). In comparison with a similar measurement of Fe-ref, these processes are occurring over a longer time period<sup>34</sup>. For instance, both sulfur samples exhibit reflections due to Fe<sub>3</sub>O<sub>4</sub> and  $\alpha$ -Fe after 4h on stream, particularly Fe-S<sub>H</sub>. Comparatively, the Fe-ref sample displays complete reduction of the iron oxide phases and formation of iron carbides within several hours of reaction<sup>34</sup>. The Fe-S<sub>H</sub> sample also exhibits a delayed onset in the formation of iron carbides, indicating that the higher loading of sulfur impedes iron oxide reduction and carbide formation.

The in situ TPO data are presented in **Figure 3(c,d)**, **Figure 5** and **Table 1**. From previous TPO analysis of the reacted Fe-ref sample, three distinct carbon oxidation peaks were identified and attributed to reactive adsorbed carbon ( $\alpha$ ), amorphous-like carbon, ( $\beta$ ) and iron carbide ( $\gamma$ )<sup>33,34</sup>. Figures 3c and 3d show all of these features are evident in the post-reaction TPO plots for the Fe-S<sub>L</sub> and Fe-S<sub>H</sub> samples.

Quantification of the TPO peak areas reveals several differences from the Fe-ref sample (**Figure 5**). Firstly, there is a delayed retention of the  $\alpha$ -peak upon the inclusion of sulfur (peak max is 6h for Fe-ref, versus 12h for Fe-S<sub>L</sub> and Fe-S<sub>H</sub>). The  $\alpha$  peak is tentatively assigned as a pre-cursor to the formation of the hydrocarbonaceous overlayer.<sup>33,34</sup> With reference to the in situ XRD analysis, the extended retention of the  $\alpha$  peak correlates with the delayed reduction of iron oxide (**Figure 4**). Secondly, the  $\beta$ -peak trends for all samples are near identical up to 12h on stream, thereafter Fe-S<sub>H</sub> begins to exhibit a distinct increase. Linking to the XRD derived deduction that the presence of sulfur impedes iron oxide reduction and carbide formation, the TPO outcomes are consistent with a constrained hydrogen supply on S doping. For example, the higher sulfur loading impedes the supply of surface hydrogen, so

that amorphous carbon formation is preferentially favoured over hydrocarbon production (methane in this case, Figures 3a and 3b).<sup>34</sup> No noticeable trends are evident in the case of the high temperature  $\gamma$  peak that is assigned to iron carbide features.

It has been previously reported that the addition of sulfur leads to a blockage of metal sites that facilitate carbidisation, perturbing iron carbide formation and instead leading to the formation of amorphous-like carbon species<sup>21</sup>. The combination of XRD and TPO data sets presented here are in agreement with this statement.

Ex situ Raman spectra of Fe-S<sub>L</sub> and Fe-S<sub>H</sub> after 6h CO hydrogenation reaction are indicative of the retention of carbonaceous species, identified as the 'D' and 'G' bands associated with disordered and ordered graphitic carbon respectively<sup>44-46</sup> (**Figure 6**).

### 3.3 Inelastic neutron scattering analysis

Previously, Warringham and co-workers have utilised INS to observe the retention of hydrocarbonaceous species on both industrially<sup>30</sup> and laboratory reacted samples.<sup>31-34</sup> It is proposed that these moieties are present in the form of an overlayer (hydrocarbonaceous and carbonaceous) which may affect the FT product distribution; the nature of both entities being dependent on the supply of hydrogen<sup>34</sup>. From the micro-reactor results reported in Section 3.2.2, the inclusion of sulfur clearly disrupts the retention of carbonaceous species, whilst perturbing the reduction of iron oxide. To investigate the potential impact on the hydrocarbonaceous species, preliminary studies of Fe-S<sub>L</sub> and Fe-S<sub>H</sub> were performed utilising the large-reactor set up located at the ISIS Facility<sup>37</sup>. It is noted that the larger sample mass and gas flows utilised in the INS experiments retard the gas exchange dynamics therefore increasing the time required to fully reduce the  $\alpha$ -Fe<sub>2</sub>O<sub>3</sub> starting phase in comparison with the micro-reactor set up. This discrepancy has been previously reported and discussed<sup>34</sup>.

**Figure 7** presents the INS spectra obtained for the Fe-ref,<sup>33</sup> Fe-S<sub>L</sub> and Fe-S<sub>H</sub> samples after 6h CO hydrogenation at 623 K, normalised to the mass of Fe. The signal-to-noise ratios for the Fe-S<sub>L</sub> and Fe-S<sub>H</sub> spectra are inferior compared to the Fe-ref spectrum due to the reduced measurement time of the two doped samples (1202  $\mu$ A h versus >2000  $\mu$ A h). However the spectral intensity observed is determined solely by the number of neutron scatters present, therefore enabling a quantitative comparison between these data sets. Evaluation of the stretching region (2000-3750 cm<sup>-1</sup>, **Figure 7a**) identifies the level of hydrocarbonaceous

species observed with the Fe-ref sample to have diminished upon inclusion of sulfur. Fe-S<sub>L</sub> and Fe-S<sub>H</sub> exhibit similar  $\nu(\text{C-H})$  features to Fe-ref at 3053  $\text{cm}^{-1}$  with a low frequency shoulder at 2932  $\text{cm}^{-1}$ . These features are respectively assigned to  $\text{sp}^2$  and  $\text{sp}^3$  hybridised C-H stretching modes. Assessment of the deformation region of the spectra (400-1600  $\text{cm}^{-1}$ , **Figure 7b**) confirms the previous observations with the Fe-S<sub>L</sub> and Fe-S<sub>H</sub> spectra being relatively featureless. The Fe-ref has previously been discussed<sup>33,34</sup> but briefly can be attributed to several aromatic  $\delta(\text{C-H})$  modes (1451, 1389 and 1160  $\text{cm}^{-1}$ )<sup>30-33</sup> alkenic  $\delta(\text{C-H})$  (953  $\text{cm}^{-1}$ )<sup>33,47</sup> an out-of-plane C-H deformation of either an olefinic or aromatic group (871 and 801  $\text{cm}^{-1}$ )<sup>48</sup>, and a C-C torsion mode of edge carbon atoms contained within a polycyclic aromatic network (506  $\text{cm}^{-1}$ )<sup>49</sup>. Despite the inability of ICP to accurately detect the sulfur content of Fe-S<sub>L</sub>, inspection of the INS spectra indicates that such a small loading is enough to perturb the distribution of the hydrocarbonaceous moieties identified for Fe-ref.

A benefit of using INS is the ability to quantify the spectral response directly with hydrogen concentration<sup>50</sup>. Quantification of the  $\nu(\text{C-H})$  signal is possible from previous calibration efforts, separating the  $\text{sp}^2$  and  $\text{sp}^3$  features<sup>39</sup>. The results are collected in **Table 2**. Interestingly, the hydrogen values of the  $\text{sp}^3$  hybridised signal at 2932  $\text{cm}^{-1}$  for Fe-ref and Fe-S<sub>L</sub> are relatively similar (*ca.* 3.30  $\mu\text{moles H g}_{\text{Fe}}^{-1}$ ) with a noticeable reduction in the  $\text{sp}^2$  hybridised signal at 3053  $\text{cm}^{-1}$ . For Fe-S<sub>H</sub> there is a significant reduction in both  $\text{sp}^3$  and  $\text{sp}^2$  hybridised features, yielding the total integrated area to be only 4.10  $\mu\text{moles H g}_{\text{Fe}}^{-1}$  in comparison to 12.81 and 9.70  $\mu\text{moles H g}_{\text{Fe}}^{-1}$  for Fe-ref and Fe-S<sub>L</sub> respectively. Due to the decreased gas exchange dynamics of the large-scale reactor the samples studied here can be placed in the earlier stages of the catalyst conditioning period during the CO hydrogenation reaction. Therefore it is suggested the reduction of the  $\text{sp}^2$   $\nu(\text{C-H})$  signal from Fe-ref to Fe-S<sub>L</sub> and the further attenuation of this moiety to Fe-S<sub>H</sub> is indicative of the delayed onset of reduction and carbidisation observed by XRD (**Figure 4**) and TPO (**Table 1, Figure 5**) upon the inclusion of the sulfur. Considering the study of Bromfield and Coville who suggest there to be, under actual FTS reaction conditions, an optimum in catalytic activity upon sulfur incorporation of *ca.* 500 ppm<sup>23</sup>, one can consider the Fe-S<sub>H</sub> sample studied here as an example of a material with a sub-optimal sulfur loading whilst the Fe-S<sub>L</sub> sample has been mildly promoted with sulfur. If one supposes that the presence of a hydrocarbonaceous overlayer is linked to FTS activity,<sup>30</sup> Figure 7 and Table 2 indicate little change in the  $\text{sp}^3$  hybridised (C-H) species for Fe-S<sub>L</sub> but a significant reduction of this entity in the case of Fe-

S<sub>H</sub>. The reduction of sp<sup>2</sup> hybridised ν(C-H) modes (olefinic/aromatic C-H moieties) is more systematic. Collectively, these trends indicate the modifier concentration to be selectively perturbing the form of the hydrocarbonaceous overlayer. Thus, it is noted that the incorporation of sulfur within the Fe-FTS catalyst matrix directly impacts the retention of hydrocarbonaceous species in a manner which correlates with reports of observed catalytic activity of sulfur promoted Fe-FTS catalysts.

The studies presented here are preliminary. FTO chemistry has only relatively recently been highlighted as a process worthy of commercial exploitation<sup>17,26</sup> and, against that background, mechanistic understanding of key stages in the process chemistry is understandably limited. Figure 7 shows that small concentrations of sulfur, known to influence short chain olefin formation,<sup>17</sup> visibly perturb formation of the hydrocarbonaceous overlayer that is linked to the more conventional FTS operation.<sup>34</sup> Specifically, it appears that the S is impeding the reduction process associated with the evolutionary phase<sup>1,31</sup> of iron based FTS catalysts. However, the ambient pressure CO hydrogenation data presented in Figure 2 is unable to discern differences in the reaction profiles of the S modified samples and to the previously reported profile for the reference material.<sup>34</sup> Hence, one is cautious to infer possible structure/activity relationships based on this dataset alone. However, given that FTO chemistry is well established under actual FTS conditions, namely elevated temperature and pressure,<sup>17</sup> future work will explore more discerning micro-reactor based reaction test conditions alongside the INS investigations. Specifically, such investigations will consider a role for the modifier constraining hydrogen supply at the catalyst surface and thereby inducing a change in the product slate from predominantly saturated products over to unsaturated products.

#### 4.0 Conclusions

Fe-FTS catalysts containing various levels of sulfur promotion were exposed to ambient pressure CO hydrogenation conditions at 623 K for specified periods of time before being characterised using in situ TPO, XRD, ex situ Raman and INS. The main findings can be concluded as follows;

- When reacted under ambient CO hydrogenation conditions for 6 h T-o-S the sulfur promoted samples exhibit nearly identical reaction profiles to that seen for the unpromoted catalyst.

- In situ XRD identifies retardation of the reduction process of the  $\alpha$ -Fe<sub>2</sub>O<sub>3</sub> catalyst upon increasing incorporation of sulfur. This in turn offsets the formation of the iron carbides in comparison to the un-promoted sample.
- In situ TPO studies indicate an increase in the formation of amorphous-like carbon species at higher sulfur loadings.
- Post-reaction INS measurements show the presence of sulfur selectively impedes the formation of a hydrocarbonaceous overlayer; differences are observed in the populations of sp<sup>2</sup> and sp<sup>3</sup> hybridised C-H entities as a function of sulfur concentration.
- Post-reaction XRD, TPO and INS provide evidence that low levels of S ( $\leq 700$  ppm) impede the availability of hydrogen at the catalyst surface.

### Acknowledgements

Sasol Ltd., the University of Glasgow and the EPSRC (grant numbers EP/P504937/1 and EP/P505534/1) are thanked for the provision of postgraduate studentships (RW and ALD). The STFC Rutherford Appleton Laboratory is thanked for access to neutron beam facilities. The Royal Society is thanked for the provision of an Industrial Fellowship (PBW).

## References

1. H. Schulz, *App.Catl.A.Gen.* 186 (1999) 3-12
2. Y. Traa, *Chem. Commun.* 46 (2010) 2175-2187
3. A.P. Steynberg, *Stud. Surf. Sci. Catal.* 152 (2004) 1-63
4. E. de Smit, B.M. Weckhuysen, *Chem. Soc. Rev.* 37 (2008) 2758-2781
5. J. van de Loosdrecht, F.G. Botes, I.M. Ciobica, A. Ferreira, P. Gibson, D.J. Moodley, A.M. Saib, J.L. Visage, C.J. Weststrate, J.W. Niemantsverdriet, *Fischer-Tropsch Synthesis: Catalysts and Chemistry*, volume 7, 525-557. Elsevier, Oxford, 2013
6. L.P. Dancuart, R. de Haan, A. de Klerk, *Stud. Surf. Sci. Catal.* 152 (2004) 472-522
7. K. Aasberg-Peterson, T. S. Christensen, I. Dybkjaer, J. Sehested, M. Ostberg, R.M. Coertzen, M.J. Keyser, A. P. Steynberg, *Stud. Surf. Sci. Catal.* 152 (2004) 248-387
8. M.E.S. Hegarty, A.M. O'Connor, J. R. H. Ross, *Catal.Today.* 42 (1998) 225-232
9. M.E. Dry, *Chemtech.* 12 (1982) 744-750
10. M. Asadullah, S. Ito, K. Kunimori, M. Yamada, K. Tomishige, *J. Catal.* 208 (2002) 255-259
11. B.H. Davis, *Ind. Eng. Chem. Res.* 46, (2007) 8938-8945
12. E.C.D. Tan, D. Schuetzle, Y. Zhang, O. Hanbury, R. Schuetzle, *Int. J. Energy Environ. Engineering*, <https://doi.org/10.1007/s40095-018-0273-9>
13. H. Arakawa, A.T. Bell, *Ind. Eng. Chem. Process Des. Dev.* 22 (1983) 97-103
14. S. Li, S. Krishnamoorthy, A. Li, G.D. Meitzner, E. Iglesia, *J. Catal.* 206, (2002) 202-217
15. M.E. Dry, T. Shingles, C.S.H. Botha, *J. Catal.* 17 (1970) 341-346
16. M.C. Ribeiro, G. Jacobs, B.H. Davis, D.C. Cronauer, A.J. Kropf, C.L. Marshall, *J. Phys. Chem. C.* 114, (2010) 7895 -7903
17. H.M.T. Galvis, A.C.J. Koeken, J.H. Bitter, T. Davidian, M. Ruitenbeek, A.I. Dugulan, K.P. de Jong, *J. Catal.* 303 (2013) 22-30
18. J. Xie, J. Yang, A.I. Dugulan, A. Holmen, D. Chen, K. P. de Jong, M.J. Louwerse, *ACS Catal.* 6 (2016) 3147-3157
19. D. Wang, J. Hi, B. Chen, W. Chen, G. Qian, X. Duan, X. Zhou, A. Holmen and S. Chen. *AIChE J.* 63 (2017) 154-161
20. B. Chen, X. Zhang, W. Chen, D. Wang, N. Song, G. Qian, X. Duan, J. Yang. D. Chen, W. Yuan, X. Zhou. *Ind. Eng. Res.* 57 (2018) 11554-11560
21. C.H. Bartholomew, R.M. Bowman, *App. Catal.* 15 (1985) 59-67
22. M.E. Dry, J.C. Hoogendoorn, *Cat. Rev – Sci. Eng.* 23 (1981) 265-278
23. T.C. Bromfield, N.J. Coville, *App. Catal. A: Gen.* 186, (1999) 297-307

24. W.L. van Dijk, J.W. Niemantsverdriet, A.M. van der Kraan, H.S. van der Braan. *App. Catal. 2* (1982) 273-288
25. H.M.T, Galvis, K.P. de Jong, *ACS Catal. 3*, (2013) 2130-2149
26. H.M.T. Galvis, J.H. Bitter, C.B. Khare, M. Ruitenbeek, A.I. Dugulan, K.P. de Jong, *Science* 335 (2012) 835-838
27. J.A. Kritzinger, *Catal.Today. 71* (2002) 307-318
28. X. Zhou, J. Ji, D. Wang, X. Duan, G. Qian, D. Chen, X. Zhou, *Chem Commun. 51* (2015) 8853-8856
29. Y. Yuan, S. Huang. H. Wang, Y. Wang, J. Wang, J. Lv, Z. Li, X. Ma. *Chem. Cat. Chem*, 9 (2017) 3144-3152
30. N.G. Hamilton, I.P. Silverwood, R. Warringham, J. Kapitan, L. Hecht, P.B. Webb, R.P. Tooze, S.F. Parker, D. Lennon, *Angew. Chem. Int. Ed.* 52 (2013) 5608-5611
31. N.G. Hamilton, R. Warringham, I.P. Silverwood, J. Kapitan, L. Hecht, P.B. Webb, R.P. Tooze, W. Zhou, C.D. Frost, S.F. Parker, D. Lennon, *J. Catal.* 312 (2014) 221-231
32. R. Warringham, N.G. Hamilton, I.P. Silverwood, C. How, P.B. Webb, R.P. Tooze, W. Zhou, C.D. Frost, S.F. Parker, D. Lennon, *App. Catal. A: Gen.* 489, (2015) 209-217
33. R. Warringham, A.R. McFarlane, P.B. Webb, R.P. Tooze, J. Taylor, D.A. MacLaren, R. Ewings, S.F. Parker, D. Lennon, *J. Chem Phys.* 143, (2015) 174703
34. R. Warringham, A.L. Davidson, , P.B. Webb, R.P. Tooze, R.A. Ewings, S.F. Parker, D. Lennon, *RSC Adv.* 9 (2019), 2608-2617
35. S.F. Parker, D. Lennon, P.W. Albers, *App. Spectrosc.* 65 (2011) 1325-1341
36. M.D. Shroff, A. K. Dayte, *Catal.Lett.* 37 (1996) 101-106
37. R Warringham, D Bellaire, S F Parker, J Taylor, R.A. Ewings, C M Goodway, M Kibble, S R. Wakefield, M Jura, M P Dudman, R P Tooze, P B Webb and D Lennon, *Dynamics of Molecules and Materials-II, Journal of Physics: Conference Series*, 554 (2014) 012005
38. P.C.H. Mitchell, S.F. Parker, A.J. Ramirez-Cuesta, J. Tomkinson, *Vibrational spectroscopy using neutrons. Series on Neutron Techniques and Applications.* World Scientific, Singapore, 2005.
39. I. P. Silverwood, N. G. Hamilton, C. J. Laycock, J. Z. Staniforth, R. M. Ormerod, C. D. Frost, S. F. Parker, D. Lennon, *Phys. Chem. Chem. Phys.* 12 (2010) 3102-3107
40. I. P. Silverwood, N. G. Hamilton, A.R. McFarlane, J. Kapitan, L. Hecht, E. L. Norris, R.M. Ormerod, C.D. Frost, S.F. Parker, D. Lennon, *Phys. Chem. Chem. Phys* 14 (2012) 15214-15225



41. D.L.A. de Faria, S.V. Silva, M.T. de Oliveira, J. Raman. Spectrosc. 28 (1997) 873-878
42. T. Herranz, S. Rojas, F. J. Pérez-Alonso, M. Ojeda, P. Terreros, J. L. G. Fierro, J. Catal. 243 (2006) 199.
43. C. H. Mejía, T. W. van Deelen, K.P. de Jong, Nat Commun. 9 (2018) 1-8
44. A. Sadezky, H. Muckenhuber, H. Grothe, R. Niessner, U. Pschl, Carbon 43 (2005) 1731-1742
45. M.A. Pimenta, G. Dresselhaus, M.S. Dresselhaus, L.G. Cancado, A. Jorio, R. Saito, Phys. Chem. Chem. Phys. 9, (2007) 1276-1291
46. F. Tuinstra, J.L. Koenig, J. Chem Phys. 53 (1970) 1126 -1130
47. I. Chamritski, G. Burns, J. Phys. Chem. B. 109, (2005) 4965-4968
48. D. Lin-Vien, N.B. Colthup, W.G. Fateley, J.G. Graselli, The handbook of infrared and Raman characteristic frequencies of organic molecules. Academic Press, Boston, 1991.
49. P.W. Albers, J. Pietsch, J. Krauter, S.F. Parker, Phys. Chem. Chem. Phys. 5 (2003) 1941-1949.
50. P.W. Albers, D. Lennon. S.F. Parker, In Neutron Scattering: Applications in Biology, Chemistry, and Materials Science, in: F. Fernandez-Alonzo, D. L. Price (Eds.), Catalysis, Elsevier, 2017, 49, pp. 279-348

**Table 1.** A comparison of the quantified peak area and temperature max from the temperature programmed oxidation studies involving samples from the Fe-S<sub>L</sub> and Fe-S<sub>H</sub> samples.

Sample	$\alpha$ peak		$\beta$ peak		$\gamma$ peak	
	C content <sup>b</sup>	T <sub>max</sub> <sup>c</sup>	C content	T <sub>max</sub>	C content	T <sub>max</sub>
<sup>a</sup> Fe-S <sub>L</sub> -3	1.30	481	9.74	593	14.79	624
Fe-S <sub>L</sub> -6	2.34	509	13.75	610	16.50	644
Fe-S <sub>L</sub> -12	3.21	516	14.56	620	20.00	649
Fe-S <sub>L</sub> -24	-	-	30.96	598	30.01	657
Fe-S <sub>H</sub> -3	1.90	485	11.58	598	9.43	627
Fe-S <sub>H</sub> -6	3.14	493	14.00	609	8.97	642
Fe-S <sub>H</sub> -12	6.42	524	26.65	613	16.87	654
Fe-S <sub>H</sub> -24	-	-	80.09	621	18.19	686

<sup>a</sup>Integer indicates total time on stream in hours, <sup>b</sup>Carbon content in mmolsc g<sub>Fe</sub><sup>-1</sup>, <sup>c</sup>T<sub>max</sub> in K.

**Table 2.** The quantified peak values for the  $\nu(\text{C-H})$  stretch features observed by inelastic neutron scattering spectra after CO hydrogenation at 623 K for 6 hours in the large-scale reactor set up.

Sample	$\nu(\text{C-H})_{2932 \text{ cm}^{-1}}$	$\nu(\text{C-H})_{3053 \text{ cm}^{-1}}$	$\nu(\text{C-H})_{\text{total}}$
Fe-ref	<sup>a</sup> 3.23	9.58	12.81
Fe-S <sub>L</sub>	3.33	6.37	9.70
Fe-S <sub>H</sub>	1.94	2.16	4.10

<sup>a</sup>Hydrogen content in  $\mu\text{mol}_{\text{H}} \text{g}_{\text{Fe}}^{-1}$

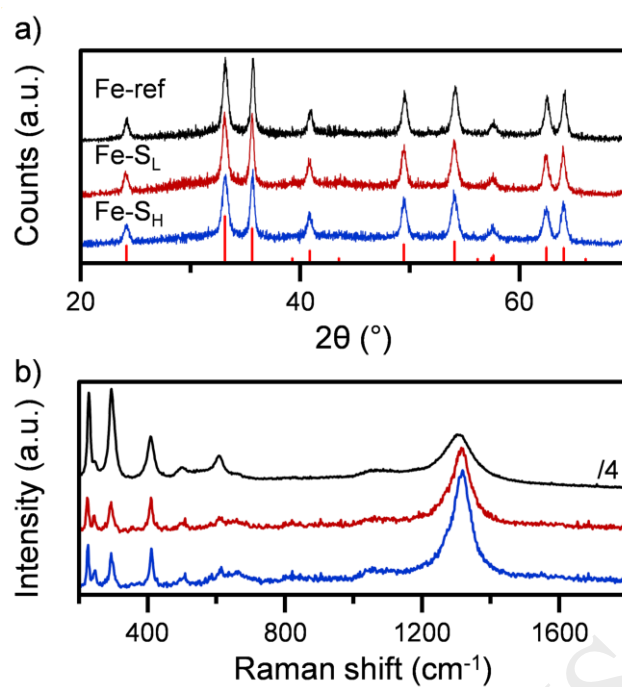


**Figure 1.** (a) Powder X-ray diffractograms and (b) Raman spectra of the freshly prepared Fe-ref (black), Fe-S<sub>L</sub> (red), and Fe-S<sub>H</sub> (blue) samples. The reference reflections of  $\alpha$ -Fe<sub>2</sub>O<sub>3</sub> are indicated by the vertical red lines. Both the diffractograms and spectra are stacked to facilitate comparison.

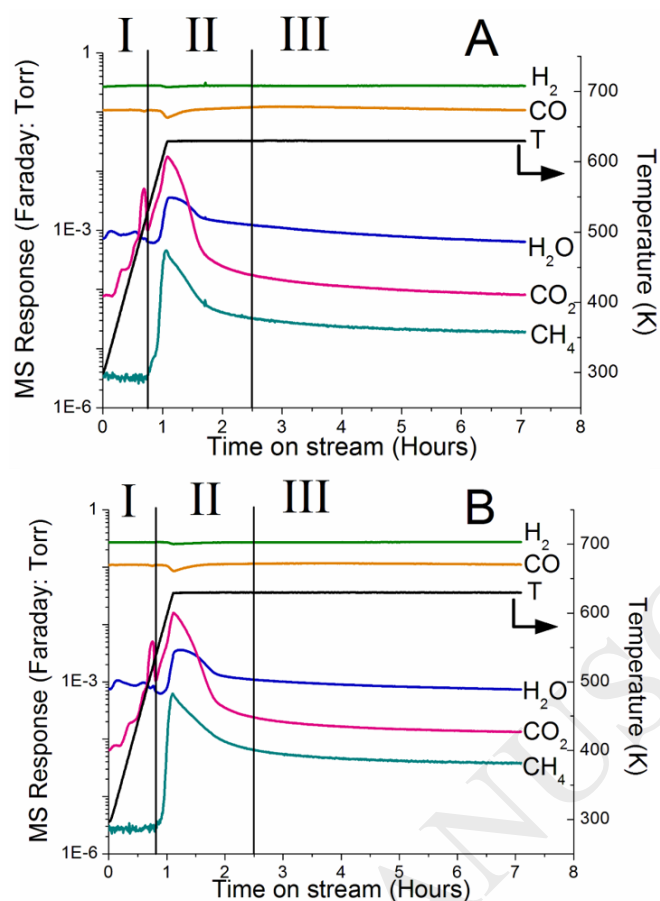


**Figure 2.** The micro-reactor reaction profile during ambient pressure CO hydrogenation at 623 K for (A) Fe-S<sub>L</sub> and (B) Fe-S<sub>H</sub>. The Roman numerals indicate the different stages present with the reaction coordinate that are described within the text.

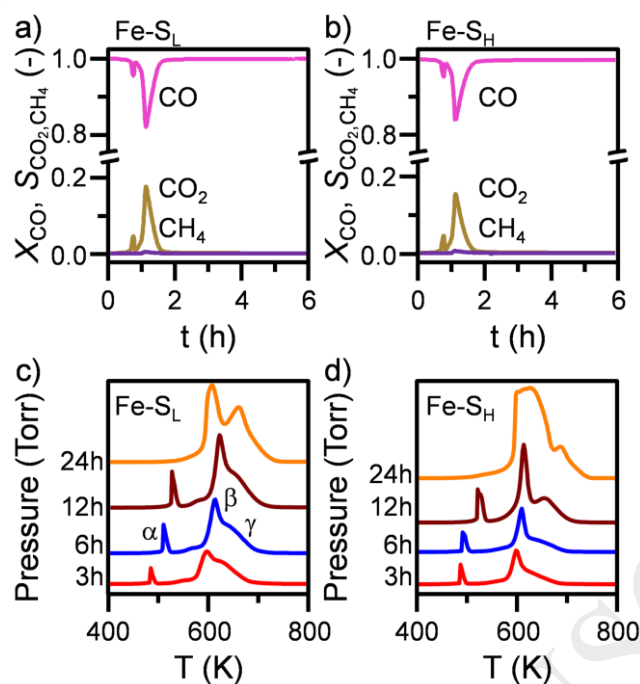


**Figure 3.** The carbon conversion and selectivity profiles for (a) Fe-S<sub>L</sub> and (b) Fe-S<sub>H</sub> during CO hydrogenation at 623 K with accompanying in situ temperature programmed oxidation profiles (c and d respectively).

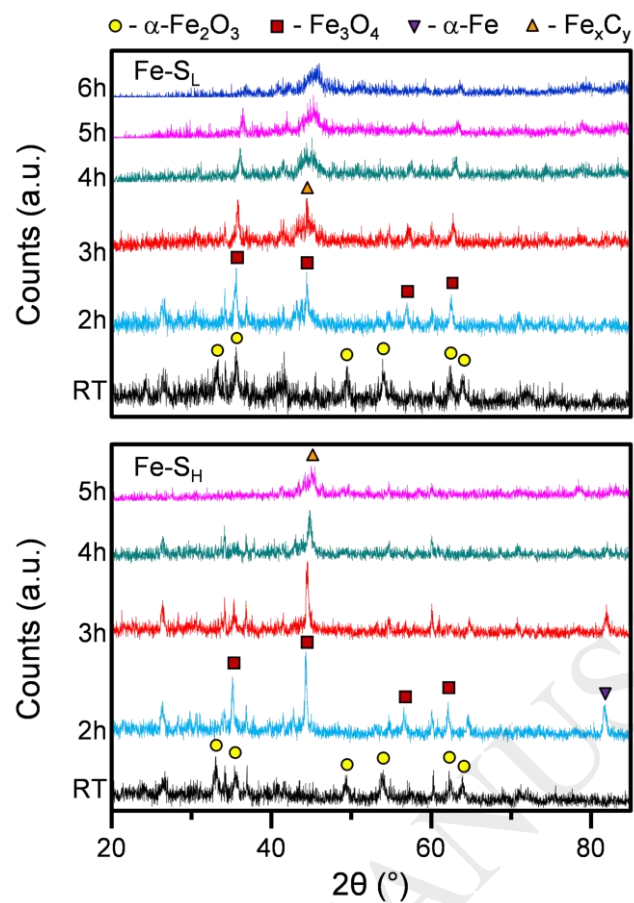


**Figure 4.** In situ X-ray diffraction study of Fe-S<sub>L</sub> and Fe-S<sub>H</sub> during CO hydrogenation at 623 K as a function of time-on-stream.

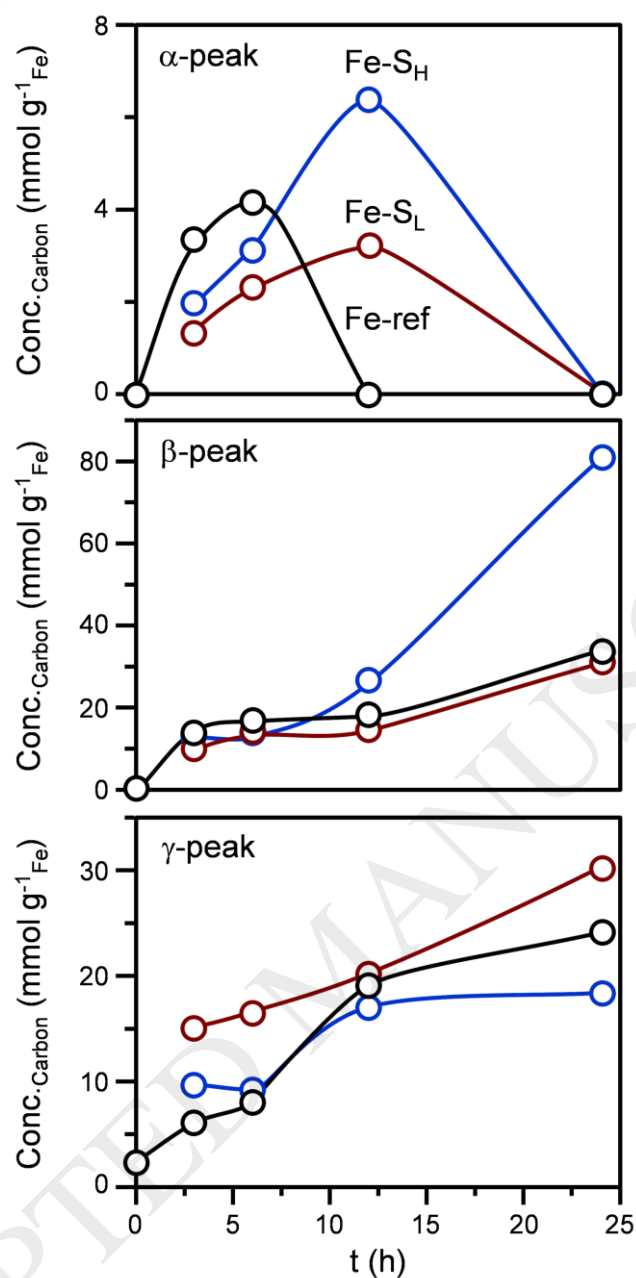


**Figure 5.** A comparison of the quantified carbon values for the  $\alpha$ ,  $\beta$ , and  $\gamma$  peaks obtained during in situ temperature programmed oxidation after CO hydrogenation at 623 K in the micro-reactor set up: Fe-ref (black); Fe-S<sub>L</sub> (brown); Fe-S<sub>H</sub> (blue).

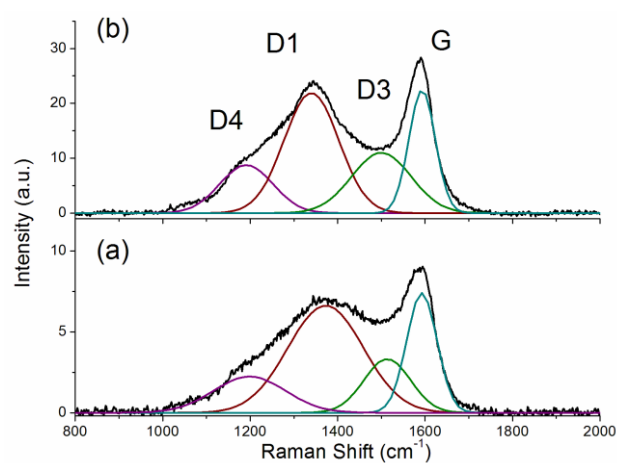


**Figure 6.** Ex situ Raman spectra of (a) Fe-S<sub>L</sub> and (b) Fe-S<sub>H</sub> after CO hydrogenation at 623 K for 6h.



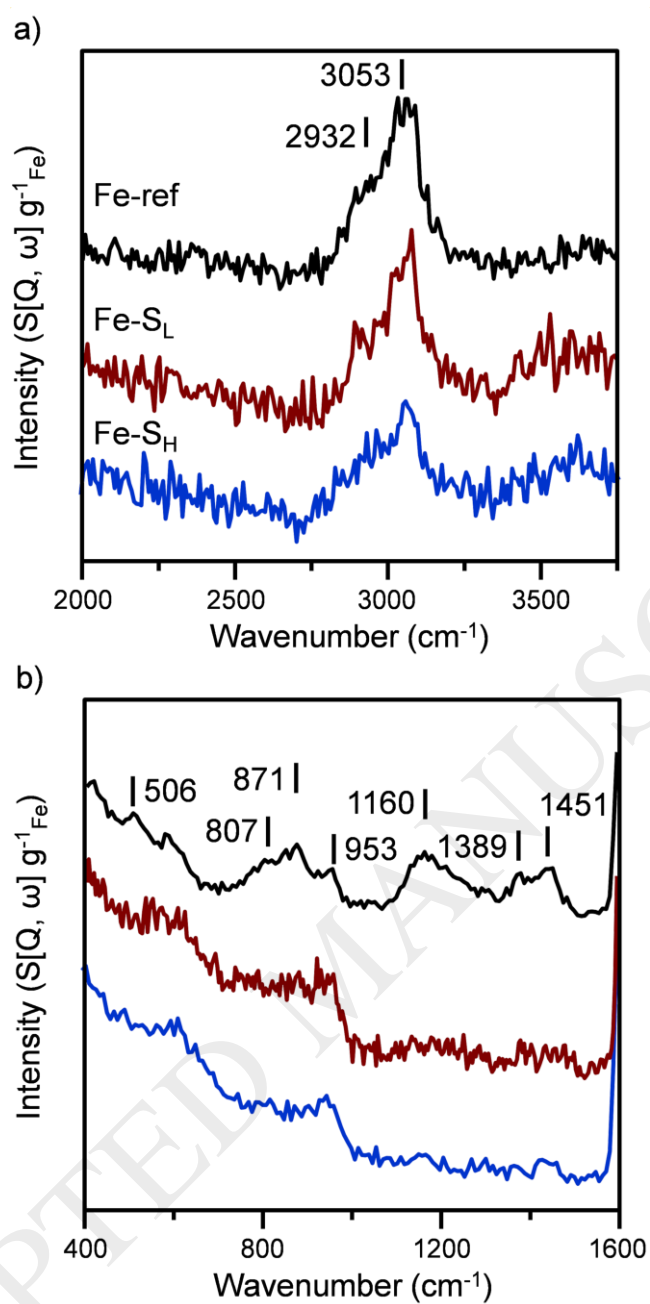


**Figure 7.** Inelastic neutron scattering spectra of Fe-ref (black), Fe-S<sub>L</sub> (brown), and Fe-S<sub>H</sub> (blue) after CO hydrogenation at 623 K for 6 h in the large-scale reactor set up: (a) 3750-2000  $\text{cm}^{-1}$ ; (b) 1600-400  $\text{cm}^{-1}$ .